Supplementary Information

Thermal Conductivity of Suspended Few-Layer MoS_2

Adili Aiyiti[1,2,3*], Shiqian Hu[1,2,3*], Chengru Wang[4*], Qing Xi[1,2,3], Zhaofang Cheng[5,6], Minggang Xia[5,6], Yanling Ma[4], Jianbo Wu[4], Jie Guo[1,2,3], Qilang Wang[1,2,3], Jun Zhou[1,2,3], Jie Chen[1,2,3], Xiangfan Xu[1,2,3], Baowen Li[7]

[1]*Center for Phononics and Thermal Energy Science, School of Physics Science and Engineering, Tongji University, 200092 Shanghai, China*

[2] *China-EU Joint Center for Nanophononics, School of Physics Science and Engineering, Tongji University, 200092 Shanghai, China*

[3]*Shanghai Key Laboratory of Special Artificial Microstructure Materials and Technology, School of Physics Science and Engineering, Tongji University, Shanghai 200092, China*

[4] *School of Materials Science and Engineering, Shanghai Jiaotong University, 200240 Shanghai, China*

[5]*Department of Optical Information Science and Technology, School of Science, Xi'an Jiaotong University, 710049 Xi'an, China*

[6] *Department of Applied Physics, School of Science, Xi'an Jiaotong University, 710049 Xi'an, China*

[7]*Department of Mechanical Engineering, University of Colorado, Boulder, CO 80309-0427, USA*

Part 1: Sample preparation and Characterization

Wet transfer method

In the main text, an obvious low thermal conductivity (the green open circles in figure 4(a)) measured on the sample prepared by wet transfer method are plotted to comparing with the ones that are fabricated by dry transfer method. The lower thermal conductivity seems reasonable due to the poor sample quality which results from the PMMA mediated fabrication process. Here, the wet transfer process is described in figure S1. First, a MoS_2 strip exfoliated from bulk crystal by Scotch tape is transferred onto the

wafer that is pre-coated with thick PMMA. The thick PMMA layer holding the sample is peeled off from the wafer and aligned to the non-suspended device under the microscope (figure S1(a)). Cr/Au (5/50nm) is deposited at the contact between the sample and membranes through standard electron beam lithography and thermal evaporation, to enhance the thermal contact (figure S1(b)). A thin layer of PMMA is spin coated on the sample, followed by another electron beam lithography, by which process the PMMA away from MoS_2 sample is etched away. The left rectangular PMMA is designed to protected MoS_2 (figure S1(c)) before the device is immersed in KOH solution to etch the silicon for suspension. At last, the suspended sample is dried in the critical point drier and annealed at 225 °C in H2/Ar atmosphere for two hours before thermal measurement. Figure S1(e-h) shows the corresponding optical images of the sample schematized in figure S1(a-d).

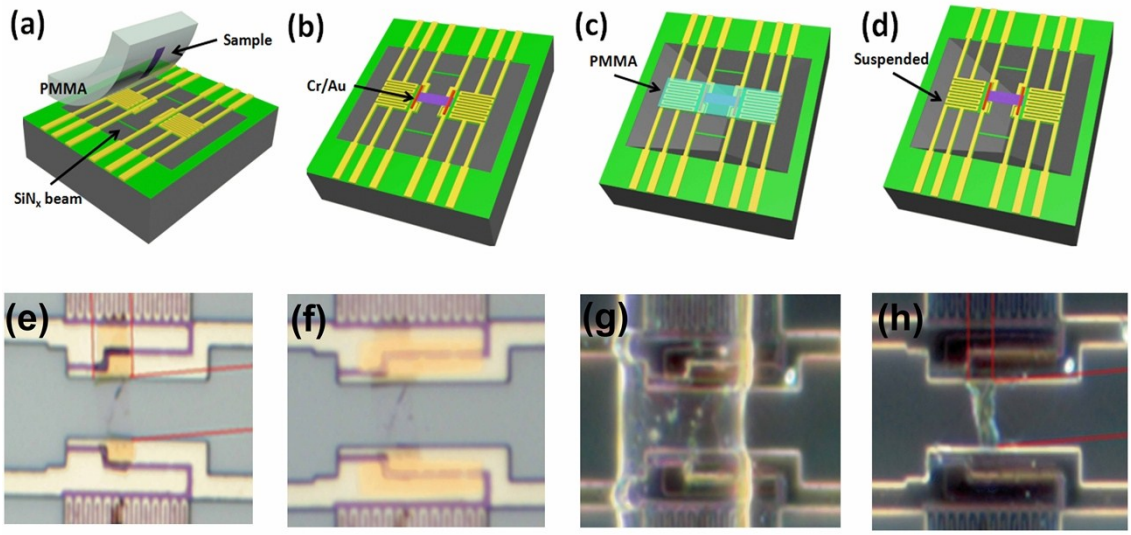

Figure S1. (a-d) Schematic of the wet transfer process. (e-h) The optical pictures of sample.

Raman spectrum and photoluminescence (PL) spectrum

Figure S2(a-c) shows the optical microscope images of the MoS_2-A, MoS_2-B and MoS_2-C. For clarity, the original data and fitting curves of the Raman spectra for MoS_2-A, MoS_2-B and MoS_2-C are shown in figure S2(d-f). The obtained difference between the E^1_{2g} peak and A_{1g} peak are 24.6 cm^{-1}, 23.9 cm^{-1} and 23.8 cm^{-1} respectively, by which the layer numbers are determined as 5, 4 and 4 layers.[1] The microscope images are snapped under the ZEISS microscope. Raman spectrum of all samples is measured after the samples are annealed at 225 °C in H_2/Ar atmosphere for two hours to clean the possible residue and contaminations.

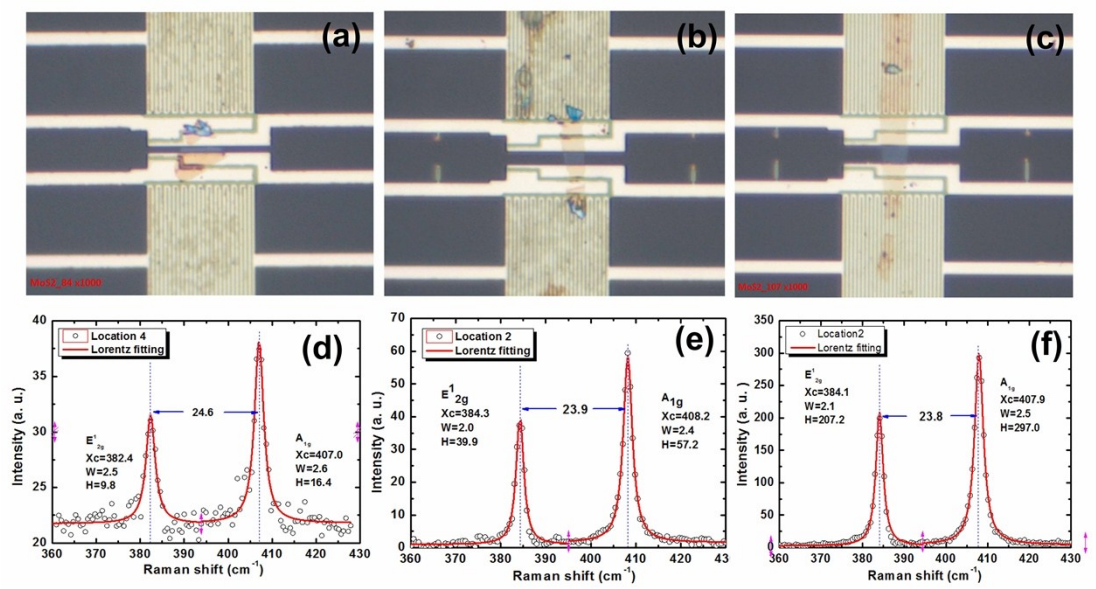

Figure S2. (a-c) Optical microscope images of the three (MoS_2-A, MoS_2-B and MoS_2-C) MoS_2 flakes on the suspended devices respectively. (d-f) Raman spectrum (before mild oxygen plasma treatment) of the corresponding samples.

The photoluminescence (PL) spectrum of MoS_2-A and MoS_2-D are shown in figure S3(c-d), whose optical microscope images are shown above (figure S3(a-b)). It can be seen clearly from the PL spectrum at different locations (supported by Pt electrodes, SiNx and totally suspended), that substrate can affect the PL emission in some manner. The emission intensities as well as the peak positions are strongly modulated by the

interference within the different substrates, which might be related to substrate-induced variations in the spectral weight and radiative decay rate of charged and neutral excitons.[2]

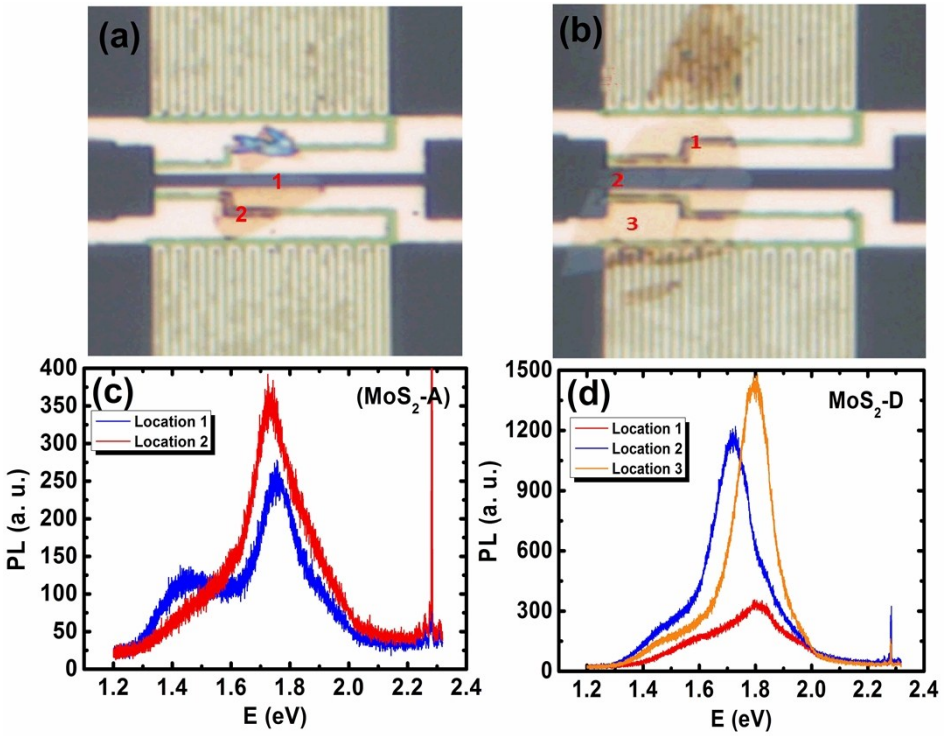

Figure S3. (a-b) The microscope images of MoS_2-A and MoS_2-D. (c-d) The corresponding PL spectrum of the samples at different locations.

Part 2: The details of measurement based on the suspended thermal bridge method

We employed the modified prepatterned suspended thermal bridge derives and similar process for thermal measurements.[3-6] A DC current is applied to generate a Joule heat which rises the temperature of R_h. The heat flux flows through the suspended sample and rises the temperature of R_s. The measured thermal conductance of the six supporting Pt/SiNx beams (G_b) and the thermal conductance of the MoS_2 samples (G_s) are written as:

$$G_b = \frac{Q_{tot}}{\Delta T_h + \Delta T_s} \tag{1}$$

$$G_s = \frac{G_b \Delta T_S}{\Delta T_h - \Delta T_s} \tag{2}$$

where Q_{tot} is total heat flow into the heater, ΔT_h and ΔT_s are the temperature rise in the heater and sensor island respectively. ΔT_h and ΔT_s are derived from the resistance changes ΔR_h and ΔR_s and the temperature coefficient of resistance (*TCR*). It is worth to note that the temperature change in each membrane as a function of applied Joule heat power is kept in the linear range during the measurement (figure S4(c)). ΔT_h and ΔT_s, are controlled to be within a few Kelvin (figure S4(c)) to minimize the possible thermal radiation between the two membranes. Generally, the measurement sensitivity of conventional thermal bridge method was in the order of 10^{-9} W/K in the past.[3] As it is also mentioned in Ref.[7, 8], when the resistance of the PRTs is measured using a lock-in amplifier in a four-probe configuration, without any optimization, the measurement sensitivity is limited to 10^{-9} W/K. In our measurements, by activating the offset and expanding function of lock-in amplifier (with an extra pre-amplifier), the lock-in resolution can be enhanced by a factor of 10 or more.[7] Furthermore, a temperature noise below 5mK (see figure S5) can be achieved by duly increasing the AC current and lock-in integral time constant in the premise of not increasing the measurement time too much, by which the measurement sensitivity could be optimized to the order of 10^{-10} W/K or more, which is enough at least in our measurement and which is actually can be further optimized by the methodology in the Ref.[9, 10] when it comes to ultra-sensitive thermal measurements. Whole thermal measurement mentioned above is carried out in

the temperature ranging from T=30K to T=305K in a variable temperature instrument (VTI) with vacuum better than 1×10^{-5} mbar and FEI SEM chamber with vacuum better than 10^{-4} Pa.

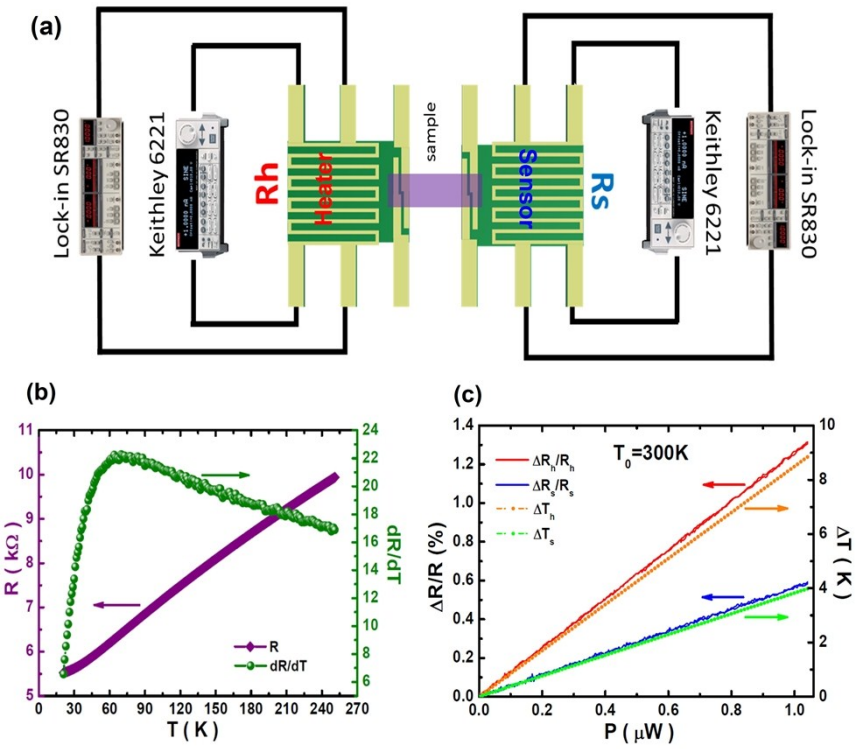

Figure S4. (a) Schematic diagram of the suspended thermal bridge method. R_h and R_s serve as heater and sensor respectively. A mixed optimized AC and DC current is supplied to the heater by Keithly 6221 and resistance of the heater is monitored by Lock-in SR830, while only an optimized AC current is applied to the sensor by Keithly 6221 and resistance of the heater is monitored by Lock-in SR830. (b) Thermometer calibration: resistance vs. temperature and the derived *TCR* values. (c) The temperature and resistance changes in the heater resistor R_h and sensor resistor R_s as a function of applied Joule heat.

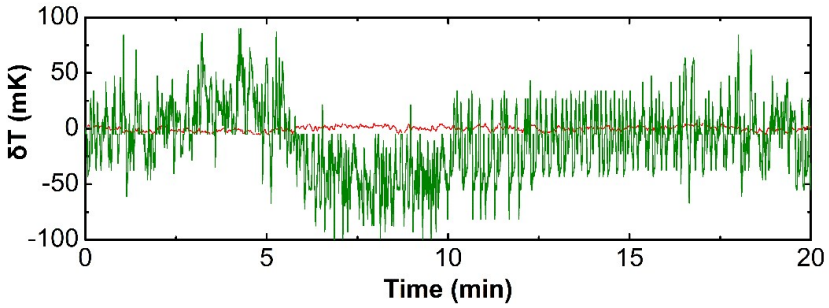

Figure S5. Sensitivity of the measurement before (green line) and after (red line) optimization

Finite Element Simulations

To simulate the temperature distribution in the suspended membranes and analysis the contact thermal resistance R_c, we carried out Finite Element Simulations (COMSOL Multiphysics 5.2, License No: 9400382). Figure S6(a) and (b) is the simulated schematic of the suspended membrane structure. Figure S6(c) shows the simulated total thermal resistance R_{tot} of a 4-layer MoS_2 with respect to the presupposed sample resistance R_s. R_{tot} can be obtained as: $R_{tot} = \frac{\Delta T_h^2 - \Delta T_S^2}{P\Delta T_S}$, where ΔT_h and ΔT_s are the average temperature rises calculated by finite element simulation. P is the heating power pass through the heater. The thermal conductivity of this four-layer sample is presupposed from 1 $Wm^{-1}K^{-1}$ to 200 $Wm^{-1}K^{-1}$ which leads to different set values of R_s. R_{tot} shows a linear dependence of R_s and the intercept indicate that the thermal contact resistance equals to 3.3×10^6 KW^{-1}， which is comparable with the result derived from the experiment. Figure S6(d) shows the temperature profile crossing the sensor at T=305K.

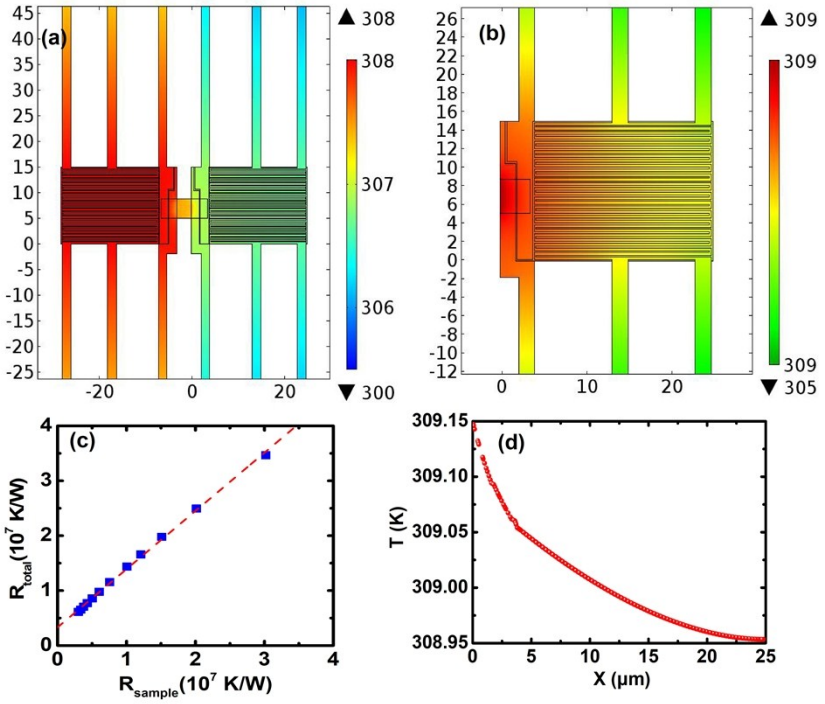

Figure S6. Finite Element Simulations (COMSOL Multiphysics 5.2) (a) Temperature distributions in heater and sensor bridged by the suspending sample at T=300 K. (b) Temperature distributions in sensor. (c) R_{total} *vs.* R_{sample} (d) Temperature profile crossing the sensor at T=305K. The inhomogeneous temperature distribution is around 0.2K, which would not affect the results much.

Part 3: Tuning the thermal conductivity by defect engineering via mild oxygen plasma

Modulation of the thermal conductivity by mild oxygen plasma is carried out in the SEM chamber by utilizing the mild oxygen plasma affiliation of the SEM. The plasma exposure parameters including pressure, exposure time are set and controlled by software automatically. So, it is possible to modulate the thermal conductivity bit by bit, though every single exposure step needs to be done very carefully. Otherwise, the samples are very easy to be destroyed by the plasma. On the other hand, after every exposure step it takes quite some time for the system to relax and recover to the same measurement condition. Thus, this is a very challenging and time-consuming process.

As supplementary for Figure 2b in the main text, 1/κ is plotted as a function of plasma exposure time (Figure S7). 1/κ increases slowly with the increasing exposure time and increases rapidly due to the occurrence of crystalline-amorphous transition before its saturation to amorphous limit. The saturation is around 65 to 75 minutes, so we normalize the plasma exposure time with 70 minutes and regard the normalized values as the defect concentration. For example, 1-minute oxygen plasma can be normalized as 1.4% defect concentration (i.e. 1/70=0.014).

After whole plasma exposure process, the samples are characterized by Raman Spectroscopy (Fig.1). Afterwards, the samples are transferred to the VTI again and thermal conductivity measurements are carried out in the temperature range of 20 K to 300 K (Fig. 4b).

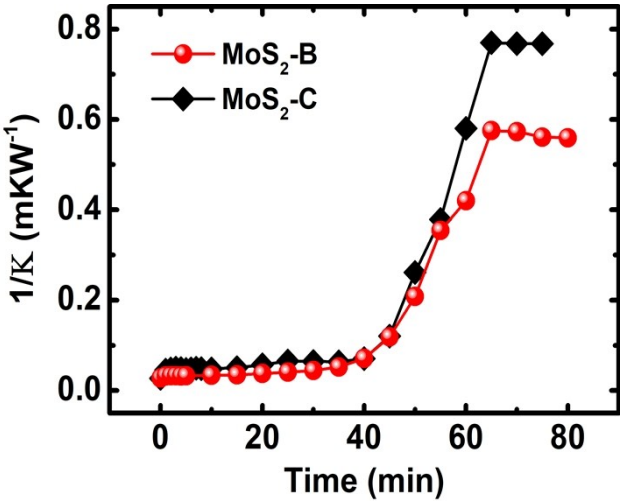

Figure S7. Reciprocal of *κ vs*. Time. The solid lines are plotted to guide the eyes.

Part 4: Molecular dynamics simulations

To establish a temperature gradient, the atoms at two ends (six layers) are coupled with Langevin heat bath at temperature T_L and T_R, respectively. The temperature gradient is

obtained by the linear fitting to the local temperature, excluding the temperature jumps at the two ends (shown in figure S8(a)). In our simulations, after the system reaching the steady state, the cumulative energy ΔE added/subtracted to the heat source/sink region are recorded for 5 ns. The time step is set as 0.5 fs. By applying the linear fitting to the raw data of the cumulative energy ΔE (shown in figure S8(b)), the energy change per unit time ($\Delta E/\Delta t$) is obtained, which is used to calculate the heat flux $J = \frac{\Delta E}{\Delta t \cdot S}$. Here S is the cross area of graphene defined as the width (W) multiplied by t thickness of MoS_2.

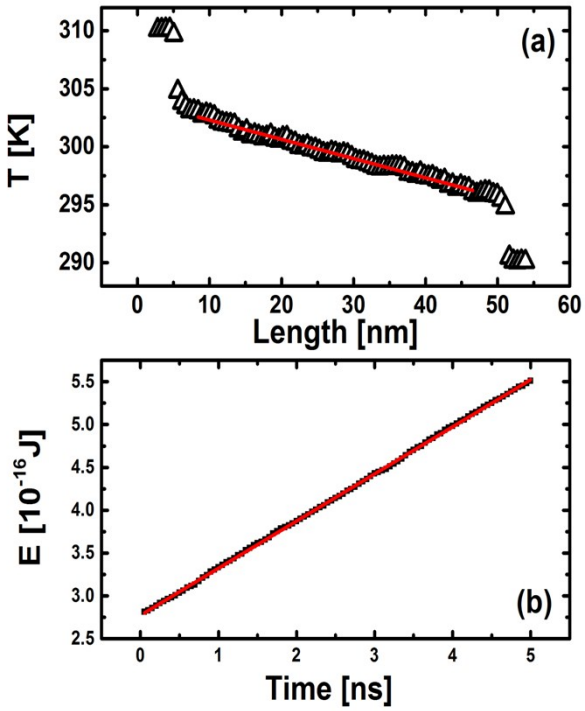

Figure S8. Temperature and heat flux calculation. (a) The typical temperature profile of the pristine MoS_2 at 300K. Linear fitting is performed to obtain the temperature gradient. (b)The typical cumulative energy change in the heat source and heat sink region for the pristine MoS_2 at 300 K. Linear fitting is performed to obtain the energy change per unit time ($\Delta E/\Delta t$), which is used to calculate the heat flux $J = \frac{\Delta E}{\Delta t \cdot S}$. Here S is the cross area of MoS_2 defined as the width (W) multiplied by the thickness.

Reference

1. C. Lee, H. Yan, L. E., T. F. Brus, Heinz, James, Hone and S. Ryu, *ACS nano*, 2010, **4**, 2695-2700.
2. M. Buscema, G. A. Steele, H. S. J. van der Zant and A. Castellanos-Gomez, *Nano Research*, 2015, **7**, 561-571.
3. L. Shi, D. Li, C. Yu, W. Jang, D. Kim, Z. Yao, P. Kim and A. Majumdar, *Journal of Heat Transfer*, 2003, **125**, 881-888.
4. P. Kim, L. Shi, A. Majumdar and P. L. McEuen, *Phys. Rev. Lett.*, 2001, **87**, 215502.
5. X. Xu, L. F. C. Pereira, Y. Wang, J. Wu, K. Zhang, X. Zhao, S. Bae, C. Tinh Bui, R. Xie, J. T. L. Thong, B. H. Hong, K. P. Loh, D. Donadio, B. Li and B. Özyilmaz, *Nat. Commun.*, 2014, **5**, 3689.
6. Z. Wang, R. Xie, C. T. Bui, D. Liu, X. Ni, B. Li and J. T. Thong, *Nano Lett.*, 2011, **11**, 113-118.
7. A. Weathers, K. Bi, M. T. Pettes and L. Shi, *Rev. Sci. Instrum.*, 2013, **84**, 084903.
8. M. T. Pettes and L. Shi, *Advanced Functional Materials*, 2009, **19**, 3918-3925.
9. S. Sadat, E. Meyhofer and P. Reddy, *Applied Physics Letters*, 2013, **102**, 163110.
10. J. Zheng, M. C. Wingert, E. Dechaumphai and R. Chen, *Review of Scientific Instruments*, 2013, **84**, 114901.